(Received 4 January 2024, Accepted 26 January 2024, Scheduled 17 February 2024)

A Miniaturized High-Selectivity Filter by Embedding Nested U-Shape Resonators in SIW

Xiaohei Yan*, Wenjing Mu, Minjie Guo, Xiumei Huang, and Haiyan Zeng

School of Mathematics, Physics, and Electronic Information Engineering
Guangxi Minzu Normal University, Chongzuo 532200, China

ABSTRACT: A substrate-integrated waveguide (SIW) miniaturization filter is proposed, which features high attenuation characteristics, effectively reduces filter loss and size, and improves frequency selectivity. The filter is miniaturized using the evanescent-mode theory and embeds a nested U-shaped resonator in the upper metal surface of the SIW. The proposed filter's equivalent circuit structure incorporates two LC parallel resonant loops with resistance characteristics that can, in turn, create two transmission zeros in the filter's stopband to enhance its selectivity. The filter has an effective size of only $0.39\lambda_g \times 0.23\lambda_g$ with a center frequency of 2.5 GHz. The -3 dB bandwidth measures 120 MHz, while the relative bandwidth is 4.8%. The insertion loss is -0.6 dB in the passband, and the return loss is more than 25 dB. Out-of-band rejection exceeds 40 dB in the range of $2.9 \sim 4.4$ GHz. The measured and simulated results agree well. The filter offers benefits in terms of high rejection, miniaturization, and low insertion loss. It can be implemented in 5G (sub-6 GHz) wireless communication systems.

1. INTRODUCTION

With the rapid development of wireless communication, filters serve as a critical frequency selection device with broad applications. Filters play a crucial role in eliminating noise and maintaining RF system stability in each link in a typical wireless transceiver system, thus having a significant impact on wireless transmission quality. To address the demands of contemporary wireless communications, scholars have extensively researched wireless communication system filters with a focus on achieving high out-of-band rejection, low insertion loss, and miniaturization.

In recent years, substrate-integrated waveguides have become commonly utilized in filter design due to their high-quality factor, low cost, low loss, and ease of planar integration [1–5]. Nevertheless, filters employing substrate-integrated waveguides present a size issue compared to other filter types. Thus, various techniques have been proposed by researchers to downsize substrate-integrated waveguide filters. The miniaturization methods commonly employed for SIW filters include $1/n$ mode cut, multilayer folding, and surface loading [6–11].

Ref. [6] controls the transmission zeros of the filter through modifications in the size of the floating disk as well as changes in the resonance mode and feed line angle, thus affording greater flexibility. However, the filter's out-of-band rejection performance is subpar. Ref. [7] proposes using square complementary split-ring resonators arranged inversely on a SIW surface to achieve filter miniaturization, yet the method's out-of-band rejection performance is not up to par. Ref. [8] reduced filter size by stacking three SIW resonators vertically and controlling transmission zero by adjusting coupling coefficients between adjacent resonators. However, the filter had significant insertion loss. Ref. [9] improved the filter quality factor by adding metal holes, but insertion loss remains large, making it difficult to meet the low insertion loss requirement in modern communication systems. Ref. [10] introduced resonators to achieve three transmission zeros in the filter's stopband, which improved the out-of-band rejection of the filter. However, this approach also increased the design complexity and size of the filter. Subsequently, [11] employed multiple modes of SIW resonant cavities to achieve a wide stopband and high selectivity. Unfortunately, the filter's insertion loss and return loss are inadequate.

The filters discussed in the literature above are unable to attain a comprehensive balance between various aspects, including high out-of-band rejection, low insertion loss, and miniaturization. Therefore, this study utilized the evanescent-mode theory of electric dipole loading to embed a nested U-shaped resonator into the upper metal surface of the substrate-integrated waveguide [12]. An innovative approach was employed to achieve a smaller filter size. Initially, a single-stage filter was designed and enhanced through the optimization of tuning using the electromagnetic simulation software HFSS. Based on the single-stage filter, a two-stage filter was successfully designed to improve passband performance and out-of-band rejection performance. The design was then processed and measured to verify its validity in reducing filter structure complexity and providing a compact solution with low insertion loss and high out-of-band rejection performance. This filter design solution is suitable for 5G (sub-6 GHz) wireless communication systems.

* Corresponding author: Xiaohei Yan (yanxiaohei@gxnun.edu.cn).

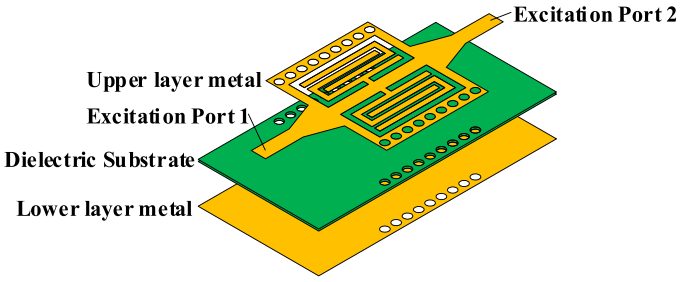

FIGURE 1. Structure of the single-stage filter.

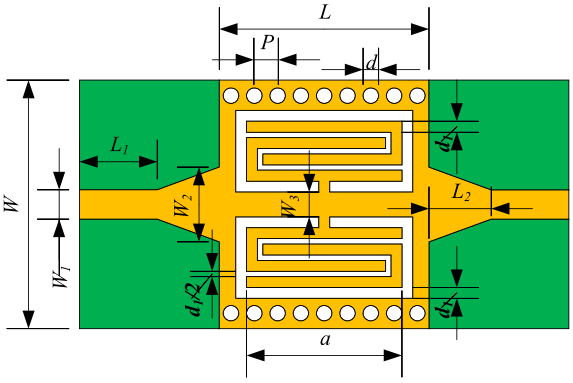

FIGURE 2. Dimensional drawing of the upper metal surface of the single-stage filter.

2. SINGLE-STAGE FILTER DESIGN

2.1. Structure of the Single-Stage Filter

The filter utilizes a single-layer substrate-integrated waveguide structure. Figure 1 displays the three-dimensional layout of the single-stage filter, which comprises two metal layers and a dielectric layer. The dielectric layer is made of ZYF300CA-P material with a relative permittivity of 3, a loss tangent of 0.0018, and a thickness of 0.762 mm. The structure involves a nested U-shaped resonator that is integrated into the upper metal surface of the substrate. The filter's input and output ports feature trapezoidal transitions for achieving impedance matching with the source or load. The upper metal surface's dimensions are visible in Figure 2. Table 1 presents the single-stage filter's optimized structural parameters following simulation analysis using HFSS software.

TABLE 1. Structural parameters of the single-stage filter (unit: mm).

$L = 13.5$	$P = 1.5$	$d = 1$	$W = 16$
$W_1 = 1.88$	$L_1 = 5$	$W_2 = 4.8$	$W_3 = 1.6$
$L_2 = 4$	$a = 10$	$d_1 = 0.7$	

2.2. Principles of Operation

The SIW is a novel waveguide structure that shares electromagnetic transmission traits with rectangular waveguides. Nonetheless, periodically spaced metalized vias located on the SIW's sidewalls obstruct the current in the figure's longitudinal propagation path, engendering a radiation effect. Consequently, the transverse magnetic wave TM mode cannot propagate via SIW. Conversely, the TE mode for a transverse electric wave comprises only a magnetic field component in the longitudinal direction of propagation and has no electric field component. As a result, the SIW can exclusively transmit TE modes, with the primary mode being TE_{10}. The cutoff frequency calculation for TE_{10} mode transmission in SIW is as follows:

$$f_c = \frac{c_0}{2W_{eff}\sqrt{\varepsilon_r}} \tag{1}$$

where c_0 is the speed of light in vacuum, ε_r the dielectric constant of the dielectric substrate, and W_{eff} the equivalent width of the SIW. The equivalent width is calculated as:

$$W_{eff} = W - \frac{d^2}{0.95p} \tag{2}$$

where W is the center distance between the two rows of circular holes on the wide side of the SIW, d the diameter of the circular holes, and p the center distance between adjacent circular holes. According to the dimensions listed in Table 1, without embedding the resonator in the SIW, the cutoff frequency of the SIW can be calculated from Eqs. (1) and (2) as:

$$f_c = 6.51\,\text{GHz} \tag{3}$$

The SIW exhibits high-pass characteristics and is suitable as a high-pass filter. To create a bandpass filter utilizing the SIW, it is essential to introduce an electromagnetic structure with bandstop characteristics into the SIW's structure. Figure 3 shows that during main mode propagation, the electric field inside the SIW is perpendicular to the upper and lower surfaces, while the magnetic field is parallel to the upper and lower surfaces. Using the theory of evanescent-mode electric dipole loading, a complementary split-ring resonator (CSRR) gap structure can be etched into the metal surface of the substrate-integrated waveguide (SIW), creating a structure with negative permeability characteristics. This generates a strong out-of-band rejection around the resonance frequency and results in the formation of a transmission zero point, which forms the passband of the filter. In this design, a nested U-shaped resonator is embedded in the upper metal surface of the substrate-integrated waveguide (SIW). This structure bears resemblance to the complementary split-ring resonator (CSRR) etched into the SIW's metal surface, allowing for the realization of a bandpass filter. The resonator's embedding also modifies the SIW's internal electric field, increasing the surface current path and resulting in a passband below the SIW's cutoff frequency. The U-shaped resonator, embedded in this design, has a longer etching gap than the CSRR, which increases the surface current path and achieves a passband lower than the cutoff frequency of the SIW, which in turn allows better miniaturization of the filter.

Figure 4 illustrates the equivalent circuit model for the single-stage filter. The upper and lower rows of metal vias in the SIW serve as a shunt inductor (L_v), providing high-pass

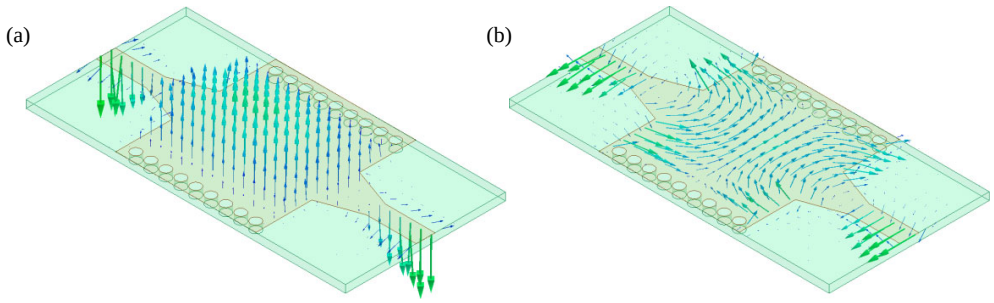

FIGURE 3. Plots of field distributions in the SIW. (a) Electric field distribution, (b) magnetic field distribution.

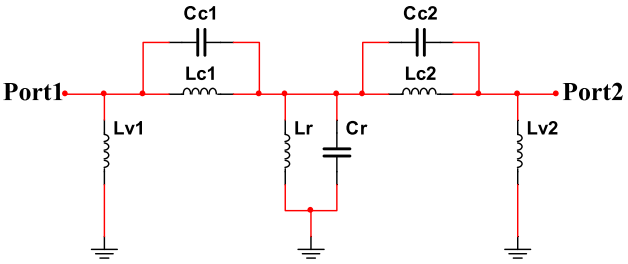

FIGURE 4. Equivalent circuit model of the single-stage filter.

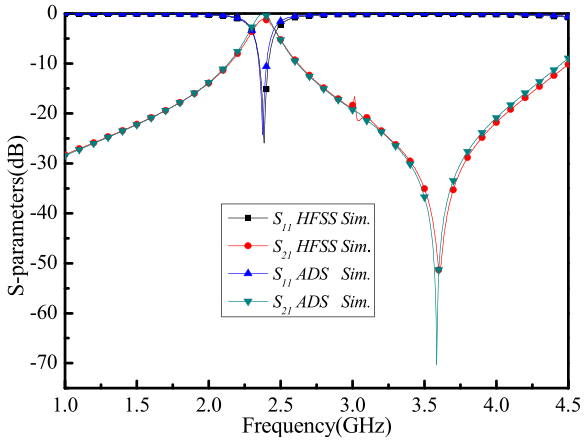

FIGURE 5. HFSS simulation results and ADS simulation results for the single-stage filter.

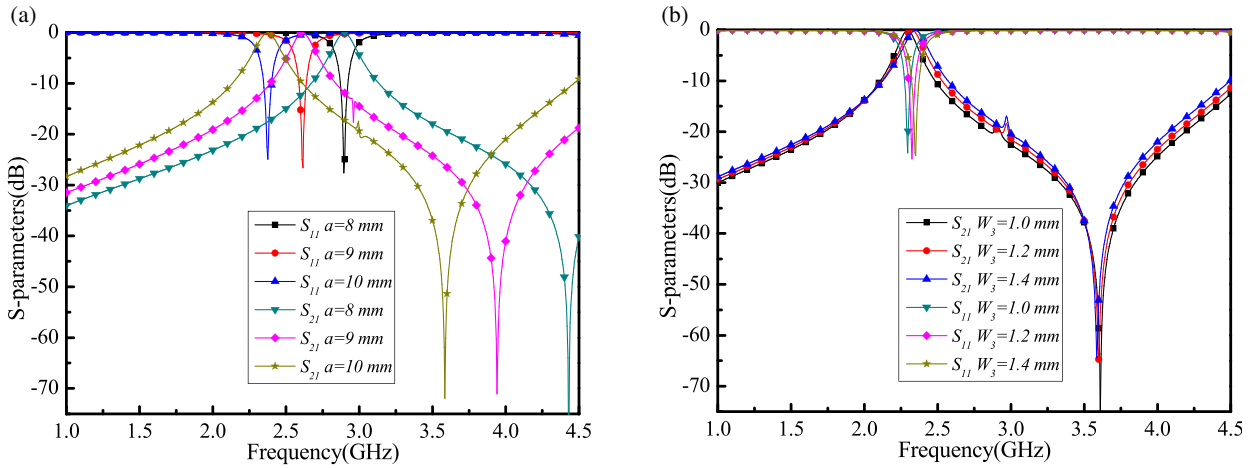

FIGURE 6. Simulation curves of S-parameters of the single-stage filter varying with different parameters. (a) Simulation curves of S-parameter variation with a. (b) Simulation curves of S-parameter variation with W_3.

characteristic. The nested U-shaped resonator, acting as a shunt resonator, is equivalent to a capacitance (C_r) and an inductance (L_r) and provides the bandpass characteristic. The SIW transmission line is connected to the nested U-shaped resonator, with L_c and C_c representing the coupling inductance and capacitance that provide the band-stop characteristic. An equivalent circuit model, simulated using ADS software, captures the actual filter's behavior, as seen in Figure 5. In the intended frequency band range, the equivalent circuit model's simulation outcomes are essentially congruent with those of the HFSS model, thus confirming the equivalence relationship.

2.3. Results and Analyses

The simulation and optimization were carried out using HFSS 15.0. The simulation curves for the S-parameters of the single-stage filter were plotted, showing their variation with different parameters in Figure 6. Figure 6(a) illustrates the simulation curves displaying variations in the S-parameters concern-

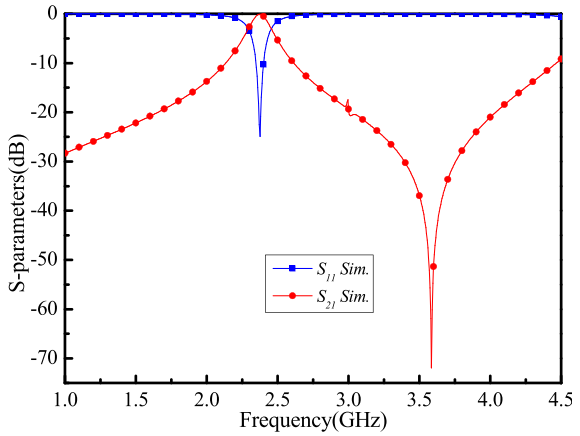

FIGURE 7. Final simulation results of the single-stage filter.

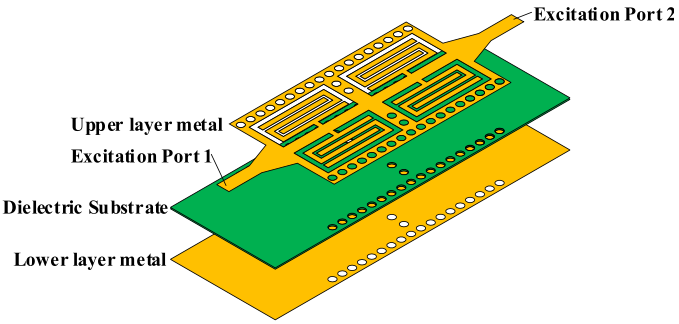

FIGURE 8. Structure of the dual-stage filter.

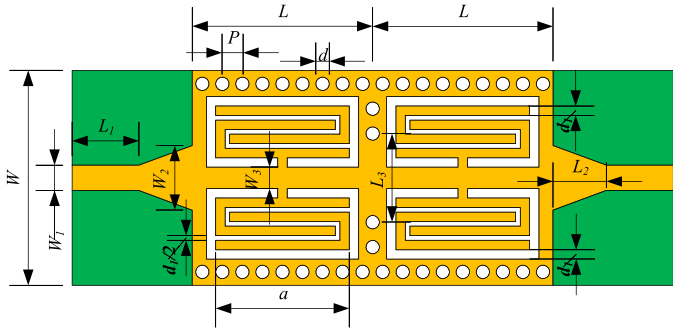

FIGURE 9. Dimensional drawing of the upper metal surface of the dual-stage filter.

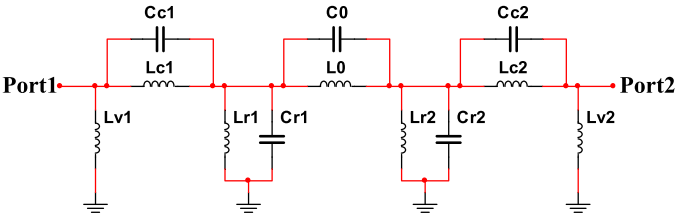

FIGURE 10. Equivalent circuit model of the dual-stage filter.

ing 'a'. The increment in 'a' leads to a decline in the center frequency and transmission zero of the filter to lower frequencies. This occurs due to an increase in the surface current path, which consequently lowers the cutoff frequency of the substrate-integrated waveguide. Increasing the value of parameter 'a' results in an increase in coupling capacitance and coupling inductance between the SIW transmission line and the nested U-shaped resonator, causing the transmission zero point to shift to a lower frequency. The S-parameter variation is illustrated in Figure 6(b), showing the center frequency of the filter moving towards higher frequencies with an increase in W_3. The reason for this is that when the W_3 is increased, the upper and lower positions of the nested U-shaped resonator deviate further from the center of the SIW. This leads to a decrease in the surface current and a resulting shift of the cutoff frequency of the SIW towards higher frequencies. Additionally, the increase in W_3 has a minimal effect on the coupling capacitance and coupling inductance between the SIW transmission line and the nested U-shaped resonator, which causes the position of the transmission zero point to remain almost unchanged.

The optimized parameters of the single-stage filter are reflected in the final simulation results, as presented in Figure 7. The filter's central frequency is significantly lower at 2.375 GHz, 63.5% below the SIW's cutoff frequency of 6.51 GHz, due to changes in the SIW's internal electric field from embedding the nested U-shaped resonator. This, in turn, increases the current paths on the metal surface of the SIW, leading to a reduced central frequency and enabling miniaturization. The bandwidth at -3 dB is 160 MHz, with a relative bandwidth of 6.7%. The filter exhibits a minimum insertion loss of -0.23 dB and a return loss greater than 25 dB. In the bandwidth range of 3–4 GHz, the out-of-band rejection is more than 20 dB. A transmission zero at 3.58 GHz with a maximum attenuation of 72 dB enhances the selectivity and out-of-band rejection performance of the filter.

3. DUAL-STAGE FILTER DESIGN

3.1. Structure of the Dual-Stage Filter

To enhance the passband performance of the single-stage filter and achieve greater selectivity, we propose a dual-stage filter based on the single-stage filter. Refer to Figure 8 for its structure. The two U-shaped resonators embedded in the metal of the SIW's upper surface are symmetrically arranged left and right. Four metal through-holes control the coupling between them, as shown in Figure 9, which depicts the surface dimensions. After optimizing the simulation using the HFSS software, Table 2 displays the dual-stage filter's final structural parameters.

TABLE 2. Structural parameters of the dual-stage filter (unit: mm).

$L = 13.5$	$P = 1.5$	$d = 1$	$W = 16$
$W_1 = 1.88$	$L_1 = 5$	$W_2 = 4.8$	$W_3 = 1.6$
$L_2 = 4$	$a = 10$	$d_1 = 0.7$	$L3 = 6.6$

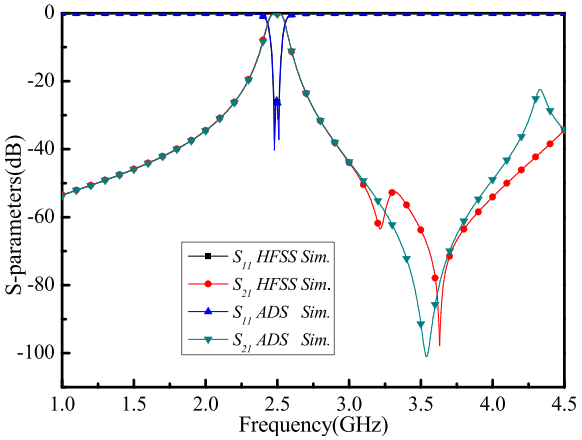

FIGURE 11. HFSS simulation results and ADS simulation results for the dual-stage filter.

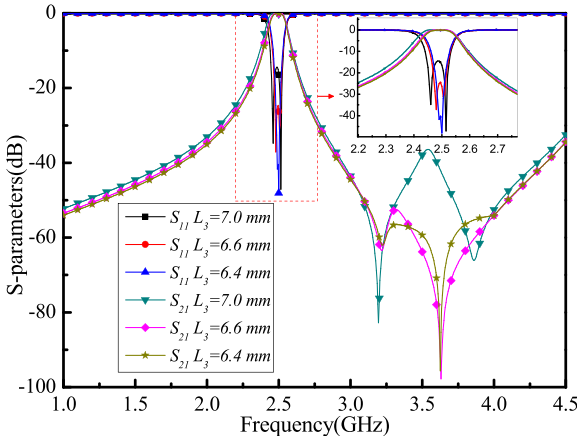

FIGURE 12. Simulation curves of S-parameter variation with L_3 value.

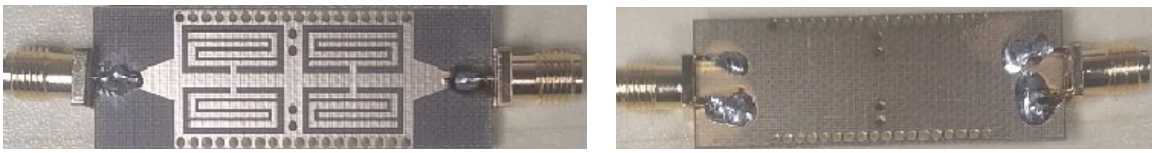

FIGURE 13. Physical picture of the filter.

3.2. Principles of Operation

As the dual-stage filter is an improvement over the single-stage filter, the corresponding circuit equivalent model must be adjusted accordingly. Figure 10 demonstrates the equivalent circuit model for the dual-stage filter. Since two nested U-shaped resonators are already embedded in the upper metal surface of the SIW, and there is an existing coupling between them, two additional pairs of resonators, namely L_{r2} and C_{r2}, and L_0 and C_0, are introduced based on the equivalent model of the single-stage filter. L_{r2} and C_{r2} refer to the shunt resonator introduced by the new nested U-shaped resonator, while L_0 and C_0 represent the coupling between the two nested U-shaped resonators. The circuit model equivalent is simulated using ADS, and the results of the simulation are displayed in Figure 11. The circuit model equivalent is largely consistent with the HFSS model simulation results within the intended frequency range, thus validating the equivalence between the two.

3.3. Transmission Response Analysis

Figure 12 displays the simulation results of the S-parameters for the filter with the value of L_3. As L_3 decreases, the filter's bandwidth narrows, and the two transmission zeros in the high-frequency direction approach each other. As L_3 decreases, the coupling between the two nested U-shaped resonators weakens, resulting in the proximal position of the two resonance frequencies in both the passband and stopband. This causes the bandwidth to narrow while transmission zeros become closer to each other. As a result, the coupling strength between the two nested U-shaped resonators determines the filter's bandwidth and the location of the transmission zeros.

3.4. Comparison of Simulation Results with Test Results

To ensure the accuracy of the design outcomes, the filter design was executed physically. Figure 13 illustrates the physical representation of the filter, where the filter's effective dimensions are 27 mm × 16 mm (excluding the input and output ports). Furthermore, the electrical length of the filter is $0.39\lambda_g \times 0.23\lambda_g$, where λ_g represents the guided wavelength at the center frequency.

Physical testing was conducted with a vector network analyzer, and Figure 14 displays the comparison between the filter's S-parameters from the simulation and its actual testing results. The simulation results show that the center frequency is 2.5 GHz, the in-band insertion loss is -0.2 dB; the return loss

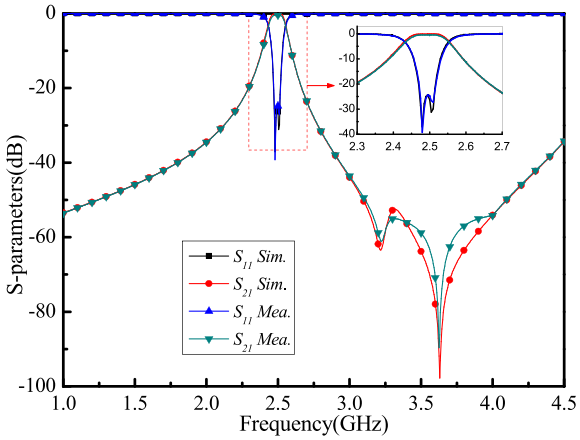

FIGURE 14. Simulation results and test results of the S-parameters of the filter.

TABLE 3. Comparison with similar filters in the literature.

Refs.	F_0 (GHz)	Insertion Loss (dB)	Return Loss (dB)	Out-of-band Suppression (dB)	Size (λ_g)
[8]	9.97	1.65	20	> 20, $12.1 \sim 19.3$ GHz	1.47×0.77
[9]	11.63	1	20	> 28, $17.3 \sim 21.3$ GHz	0.82×0.82
[10]	13.53	1.12	16.73	> 20, $13.1 \sim 13.9$ GHz	0.84×0.84
[11]	8.98	0.9	20	> 20, $11.5 \sim 11.8$ GHz	1.23×1.23
This work	2.5	0.6	25	> 40, $2.9 \sim 4.4$ GHz	0.39×0.23

is more than 25 dB; the -3 dB bandwidth is 120 MHz; the relative bandwidth is 4.8%; the out-of-band rejection is more than 40 dB in the frequency band range of $2.9 \sim 4.4$ GHz; the two transmission zeros are located at 3.22 and 3.63 GHz; and the maximum attenuation is 97.76 dB. The test results show that the center frequency of the filter is 2.5 GHz; the insertion loss is only -0.6 dB; the return loss is more than 25 dB; and the out-of-band rejection also achieves the expected target. Some discrepancies between the test and simulation results are caused by joint loss and soldering errors. However, the test results are in good agreement with the simulation ones, and the validity of the design is well verified.

Table 3 compares the performance parameters of the two-stage filter designed in this study with those of other filters in the literature. The results indicate that our filter has significant advantages concerning insertion loss, return loss, and out-of-band rejection, as well as a smaller size.

4. CONCLUSION

In this study, we have utilized the evanescent-mode theory to design a highly selective miniaturized SIW filter. The filter size has been reduced significantly to 27 mm $\times$ 16 mm ($0.39\lambda_g \times 0.23\lambda_g$) while maintaining exceptional performance. The center frequency of the filter is 2.5 GHz, with a mere insertion loss of 0.6 dB. The return loss is measured to be more than 25 dB, and the out-of-band rejection achieves more than 40 dB within the frequency band of 2.9–4.4 GHz. The transmission zeros are situated at 3.22 and 3.63 GHz, and the maximum attenuation reaches 97.76 dB. The test results agree well with the simulation ones, providing further evidence of the effectiveness of this design. The filter features low insertion loss, high out-of-band rejection, and miniaturization, making it suitable for potential applications in 5G (sub-6 GHz) communication systems.

ACKNOWLEDGEMENT

This work is supported by the Chongzuo Science and Technology Program Project (No. 2023ZC025654), the School-level Research Project of Guangxi Minzu Normal University (No. 2022SP007), the Basic Research Ability Improvement Project for Young and Middle-aged Teachers in Guangxi Universities (No. 2023KY0793 and No. 2023KY0796), and the Guangxi Natural Science Foundation (No. 2022JJB150010).

REFERENCES

[1] Bozzi, M., A. Georgiadis, and K. Wu, "Review of substrate-integrated waveguide circuits and antennas," *IET Microwaves, Antennas & Propagation*, Vol. 5, No. 8, 909–920, Jun. 2011.

[2] Chen, X.-P. and K. Wu, "Substrate integrated waveguide filter: Basic design rules and fundamental structure features," *IEEE Microwave Magazine*, Vol. 15, No. 5, 108–116, 2014.

[3] Moscato, S., C. Tomassoni, M. Bozzi, and L. Perregrini, "Quarter-mode cavity filters in substrate integrated waveguide technology," *IEEE Transactions on Microwave Theory and Techniques*, Vol. 64, No. 8, 2538–2547, Aug. 2016.

[4] Jones, T. R. and M. Daneshmand, "Miniaturized folded ridged half-mode and quarter-mode substrate integrated waveguides for filter design," *IEEE Transactions on Microwave Theory and Techniques*, Vol. 67, No. 8, 3414–3426, Aug. 2019.

[5] Qin, R., D. Zhang, Z. Ding, and M. Wang, "Duel-band filter with high out-of-band rejection using ACSRR-SIW technology," *IEICE Electronics Express*, Vol. 17, No. 12, 20190743, Jun. 2020.

[6] Liu, Q., D. Zhou, J. Shi, and T. Hu, "High-selective triple-mode SIW bandpass filter using higher-order resonant modes," *Electronics Letters*, Vol. 56, No. 1, 37–39, 2019.

[7] Zhang, X. and M. Yu, "A SIW filter with square complementary split-ring resonators (CSRRs)," in *2017 USNC-URSI Radio Science Meeting*, 45–46, IEEE, NY, USA, Jul. 2017.

[8] Shen, W. and H.-R. Zhu, "Vertically stacked trisection SIW filter with controllable transmission zeros," *IEEE Microwave and Wireless Components Letters*, Vol. 30, No. 3, 237–240, 2020.

[9] Delmonte, N., M. Bozzi, L. Perregrini, and C. Tomassoni, "Miniaturized SIW filters based on shielded quarter-mode cavities," in *2019 IEEE MTT-S International Conference on Numerical Electromagnetic and Multiphysics Modeling and Optimization (NEMO)*, 1–3, IEEE, NY, USA, May 2019.

[10] Guo, H., X. An, and Z.-Q. Lv, "Dual-mode bandpass substrate integrated waveguide filter with a complementary split ring resonator," *Microwave and Optical Technology Letters*, Vol. 60, No. 3, 735–741, Mar. 2018.

[11] Liu, J.-P., Z.-Q. Lv, and X. An, "Compact substrate integrated waveguide filter using dual-plane resonant cells," *Microwave and Optical Technology Letters*, Vol. 58, No. 1, 111–114, Jan. 2016.

[12] Danaeian, M., A.-R. Moznebi, and K. Afrooz, "Super compact dual-band substrate integrated waveguide filters and filtering power dividers based on evanescent-mode technique," *AEU-International Journal of Electronics and Communications*, Vol. 125, 153348, Oct. 2020.